Bulgarian Chemical Communications, Volume 50, Special Issue J (pp. 270–280) 2018

Structural and chemical evolution of mineral forms of tungsten in the oxidation zone of the Grantcharitza deposit (Western Rhodopes, Bulgaria)

M. P. Tarassov*, E. D. Tarassova

Institute of Mineralogy and Crystallography "Acad. Ivan Kostov", Bulgarian Academy of Sciences, Acad. Georgy Bonchev Str., bl. 107, 1113 Sofia, Bulgaria

Received March, 2018; Revised June, 2018

Two principal trends of structural and chemical evolution of mineral forms of W are distinguished in the oxidation zone of the Grantcharitza tungsten deposit. The first trend concerns the processes that occur when the overall pH of supergene solutions decreases. The first group of processes include: (1) dissolution of scheelite, $CaWO_4$, accompanied by the formation of polytungstate ions in the solution at pH ~6–4; (2) pseudomorphic replacement of scheelite by poorly crystalline $WO_3.xFe_2O_3.nH_2O$ (iron-containing meymacite) at pH ~4–1; (3) crystallization of tungstite, $WO_3.H_2O$, and hydrotungstite, $WO_3.2H_2O$, at the expense of meymacite at pH <1. The second group of processes proceeds in the overall trend of increasing pH of supergene solutions and includes: (1) partial dissolution of meymacite upon increasing the pH and the K, Na and W content in the solution (pH ~1–3); (2) occasionally, precipitation of amorphous gels $WO_3.xFe_2O_3.nH_2O$ – chemical counterparts of meymacite (pH ~1–3); (3) crystallization of hydrokenoelsmoreite, $(W,Fe)_2(O,OH)_6.H_2O$ – the second chemical counterpart of meymacite with the pyrochlore structure type, as result of the interaction of meymacite and solution enriched with K, Na, Ca and, most probably W, at pH ~3–4; (4) formation of mineral bearers of W: goethite, α-FeOOH, hematite, α-Fe_2O_3, undefined amorphous $SiO_2.xAl_2O_3.yFe_2O_3.nH_2O$ gels, and, rarely, of $CaWO_4$, and stolzite, $PbWO_4$, at pH>4. It is shown that the increase of pH from <1 to 4 causes the successive change of the structure types: ReO_3 (ReO_3-type layers in the structures of tungstite and hydrotungstite), hexagonal tungsten bronze (HTB) (HTB-type layers in the structure of $WO_3.1/3H_2O$, meymacite), and pyrochlore (structure of hydrokenoelsmoreite).

Keywords: scheelite alteration, oxidation zone, secondary tungsten minerals, structure types.

INTRODUCTION

In 1981, Th. G. Sahama in his review [1] devoted to the secondary W minerals wrote that "The secondary tungsten minerals form a group of species with no crystallographic interrelationship". For the decades since then, new data on the secondary W minerals were collected and a number of new secondary W minerals with simplified formula $(W,Fe)(O,OH)_3.nH_2O$ (hydrokenoelsmoreite, pittongite) were discovered [2–4]. Several new phases of $WO_3.nH_2O$ (1/3, 1/2) with structures of hexagonal tungsten bronze and pyrochlore were synthesized using the soft chemistry (chemie douce) approach [5]. These new phases have their natural analogues as hydrokenoelsmoreite with a pyrochlore type of structure [2] and poorly crystalline $WO_3.1/3H_2O$ [6]. The obtained so far data show that the structures of the secondary W minerals of the type $(W,Fe)(O,OH)_3.nH_2O$ and their artificial counterparts have similar structure elements such as layers of hexagonal tungsten bronze or/and ReO_3 perovskite [5]. Such minerals as pittongite and phyllotungstite [3, 4] are characterized with combined pyrochlore and tungsten bronze types of structure.

Thus, the crystallographic interrelationships between the secondary W minerals do exist. However, it is difficult to relate these minerals and their structure to certain physicochemical conditions. The synthesis conditions can hardly be used directly to interpret the natural conditions as they depend on numerous geological factors.

The processes of weathering occurring in W deposits cause a significant change in the mineral composition and properties of W ores, which makes them unsuitable for flotation and gravity beneficia-

* To whom all correspondence should be sent:
E-mail: mptarassov@gmail.com

tion. The behavior of W in the oxidation zone is very complicated due to complex aquatic chemistry of the element and its ability to polymerize. Recently, W has become the subject of scientific focus due to the possible toxicity of W in drinking water [7]. Weathering of W deposits is considered as one of the possible sources of W in ground waters [8].

The processes of weathering affect significant part of the Grantcharitza deposit (Western Rhodopes), the largest tungsten deposit in Bulgaria. In the present paper, the authors discuss the principal features of the development of the oxidation zone in the Grantcharitza tungsten deposit and the structural and chemical evolution of different secondary mineral forms of W by connecting them with certain physicochemical conditions.

BREAF INFORMATION ABOUT THE GRANCHARITSA DEPOSIT

The Grantcharitza tungsten deposit is situated in the Western Rhodopes Mountains, 18 km southwest of the town of Velingrad (Plovdiv region, Bulgaria). The deposit is localized in porphyritic biotite granites and amphibole-biotite granodiorites of the so-called "unit 1" of the composite Rila-Western Rhodopes Batholith [9]. The ore mineralizations occur in pegmatoid quartz-feldspar veins characterized by almost sub latitudinal strike – dipping to NW ~350° with slope of ~30° and in the wall-rock as vein-disseminated ores ("mineralized granitoids"). The mineral composition of the vein ores is characterized by strong domination of quartz, SiO_2, and potassium feldspar, $KAlSi_3O_8$ (microcline) among the gangue minerals and of pyrite, FeS_2, and scheelite, $CaWO_4$, among the ore minerals. The region of the deposit is characterized by broken terrain which causes fragmentariness of the weathering crust. The oxidation zone of the deposit is developed unevenly. Most intensive supergene processes are observed in the southern upper area of the most economically important Grantcharitza-Center section of the deposit. There, a significant part of the relief is presented by a gentle slope (~30°) of the Grantcharitza River valley. This slope is subparallel to the ore zone and thus ensures nearly even access to the ore zone of the weathering agents – water, atmospheric oxygen, microorganisms, etc. The textural and structural features of the primary ores and their mineral composition (presence of quartz and potassium feldspar which screen the ore minerals from the weathering agents) contribute to the inhomogeneous development of the supergene processes which are controlled by the fracture zones in the ores.

The most important supergene process that ultimately modifies the primary ores is the oxidation of pyrite and the generation of natural sulfuric acid. Goethite, α-FeOOH, and jarosite, $KFe_3(SO_4)_2(OH)_6$, are two most dominated minerals in the oxidation zone of the deposit indicating very high variation of pH of the supergene solution – from neutral to strongly acid, and Eh being very close to the values typical for waters being in direct contact with atmospheric oxygen [10]. All altered ores in the oxidation zone are clearly divided into two groups: limonitized ones with dominated ferric iron oxides/oxyhydroxides and non-limonitized ones, containing jarosite and a variety of secondary tungsten minerals.

MATERIAL AND METHODS

Representative samples from a personal collection of the authors taken from the oxidation zone of the Grantcharitza deposit (Center section) are used for the present study. Scanning electron microscopy and electron probe microanalysis (Philips SEM515 – WEDAX3A and ZEISS EVO LS25 – EDAX Trident) at 15–20 kV acceleration voltage, and micro-Raman spectroscopy (MicroDil 28 (Dilor Co.) with an Olympus 100x microscope objective, 488-nm line of an Ar^+ laser, laser power below 2 mW at the sample surface) were the main methods for the sample characterization. For a part of the samples, transmission electron microscopy (Philips TEM420) at 120 kV and Powder X-Ray diffraction analysis (DRON-UM1, CoKα and CuKα radiations) were also applied. For better understanding the supergene processes in the oxidation zone of the deposit, the authors have constructed series of Eh–pH diagrams for the systems W–Ca–Fe–S–K–O–H and W–Fe–O–H at 298 K and 1 atm. using the thermodynamic data from [11–13] and the activities of chemical components (ΣFe – 10^{-4}, Ca^{2+} – 10^{-4}, ΣS – 10^{-2}, K^+ – 10^{-3}) in aqueous solutions typical for the oxidation zones of ore deposits [10, 14]. The thermodynamic activity of W for the system W–Fe–O–H was chosen equal to 10^{-5} – the value corresponding well to the $CaWO_4$ solubility in water according to [15]. For simplification, only the monomeric tungstate ion [WO_4^{2-}] was taken into account.

RESULTS AND DISCUSSIONS

The following W minerals and W-bearing minerals are established in the oxidized ores: (i) hypogene minerals – scheelite $CaWO_4$ (intact and relic – most common); (ii) supergene minerals: iron-containing meymacite $WO_3.xFe_2O_3.nH_2O$ (important), tungstate $WO_3.H_2O$, hydrotungstite $WO_3.2H_2O$,

iron-containing hydrokenoelsmoreite (ferritungstite) $(W,Fe)_2(O,OH)_6.H_2O$, stolzite $PbWO_4$ (rare), colloform supergene scheelite $CaWO_4$ (rare), amorphous $WO_3.xFe_2O_3.nH_2O$ gels; (iii) mineral bearers of tungsten: goethite α-FeOOH (most widespread), hematite α-Fe_2O_3, amorphous $SiO_2.xAl_2O_3.yFe_2O_3.nH_2O$ gels.

Scheelite, $CaWO_4$, (endogenic) is the most important mineral form of W in the oxidized ores. The mineral is represented by: (1) intact crystals (most spread from), (2) crystals with pronounced signs of dissolution without formation of secondary minerals (wide spread form), and (3) relic forms replaced by secondary W mineral, $WO_3.xFe_2O_3.nH_2O$. The case (2) is shown in Fig. 1: the most intensive dissolution of the scheelite crystals takes place along the {101} crystallographic planes corresponding to the cleavage planes. The development of the dissolution process along {101} causes the formation of etch hillocks and pits with {101} faces and large empty channels along [001].

The calculated concentration of W in aqueous solution as a result of equilibrium dissolution of $CaWO_4$ ($CaWO_4$=Ca^{2+}+WO_4^{2-}, ΔGr (298) = +50.16 kJ; thermodynamic data are from [11]) is equal to $4\cdot10^{-5}$ m (~$4\cdot10^{-5}$ M or 7.4 mg/L) and well corresponds to the experimental data of [15]. This value exceeds the highest concentration of W (10^{-5} M) in an aqueous solution that contains only monomeric ion and molecular W forms [16] thus indicating that the polymeric forms of W should play a significant role in the interaction scheelite – supergene solution. According to [15] at pH < 6 the concentration of W in the aqueous solution in contact with scheelite becomes notably higher than that in the neutral solutions as a sequence of the increased role of polymeric forms of W as paratungtstate-B $[H_2W_{12}O_{42}]^{10-}$, α-metatungstate $[H_2W_{12}O_{40}]^{6-}$ and other isopolytungstate ions. The role of monomeric forms of tungsten WO_4^{2-} is significant at pH>6. These data show that, at least at the beginning stages of scheelite alteration, at pH<6 to about 4 the only process of changing the mineral is its dissolution which proceeds with the formation of polytungstate ions. These ion forms of W are able to be transported over long distances in a supergene solution. The speciation of tungsten in aqueous solutions is expected to be more complex in the presence of Fe, Al, Si and P (typical for supergene solutions) due to the formation of tungsten heteropolyanions [17].

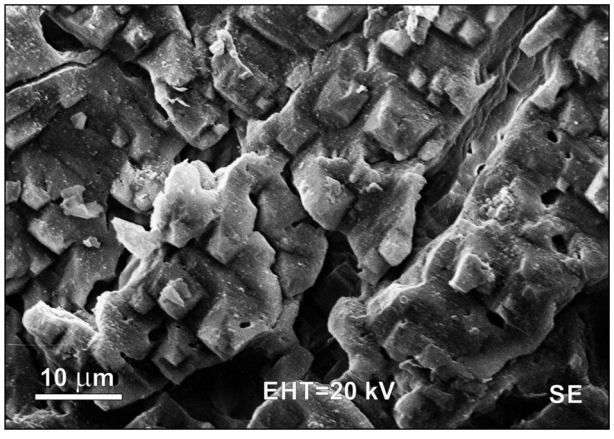

Fig. 1. Natural dissolution of scheelite, $CaWO_4$, in the oxidation zone of the Grantcharitza deposit. {101} faced hillocks and pits and channels along [001] are formed.

The second type of scheelite alteration in the Grantcharitza deposit is illustrated in Fig. 2: the mineral is pseudomorphically replaced by the secondary $WO_3.xFe_2O_3.nH_2O$ product (iron-containing meymacite or iron-containing ochre) in the acid medium of the oxidation zone enriched with Fe ions. The replacement is crystallographically controlled by the {101} cleavage planes of scheelite (Fig. 2b). The two fields ($WO_3.H_2O$ + α-FeOOH) and ($WO_3.H_2O$ + $KFe_3(SO_4)_2(OH)_6$) in the Eh-pH diagram (Fig. 2c) appear to reflect realistically the conditions of the alteration of scheelite and the formation of $WO_3.xFe_2O_3.nH_2O$, since the boundaries in the diagram between the W phases are independent of the type and concentration of the dissolved W species.

Iron-containing meymacite (ochre), $WO_3.xFe_2O_3.nH_2O$, is the most widespread supergene mineral of W in the deposit and the earliest product of scheelite alteration, and occurs as full or partial pseudomorphs after scheelite (Figs. 2a, b; 3a). The material has a glassy appearance and color in different nuances of yellow and brown – from light-yellow to dark- and black-brown. In the formula $WO_3.xFe_2O_3.nH_2O$ of the iron-containing meymacite, the coefficient *x* varies in the range 0.12–0.25 (~0.15 is the most common) and positively correlates with the coefficient *n* for water molecules varying in the range 1.8–3.9. The content of iron correlates with the color of the material: a higher content of iron corresponds to a darker color. All varieties of meymacite are poorly crystalline: their XRD patterns consist of two distinct peaks at 3.85 and 1.925 Å and asymmetric amorphous halos.

The performed observations reveal that all varieties of iron-containing meymacite are derivatives/modifications of the earliest variety of meymacite with Fe/W atomic ratio equal to ~0.2. The modification of the earliest meymacite includes also the textural changes of the material as a result of the aging processes (aging of gels) [18]. The results of the aging process are shown in Fig. 3a and b: the material consists of two parts – glassy massive one (a) and spongy aggregates (b) in the cavities of the

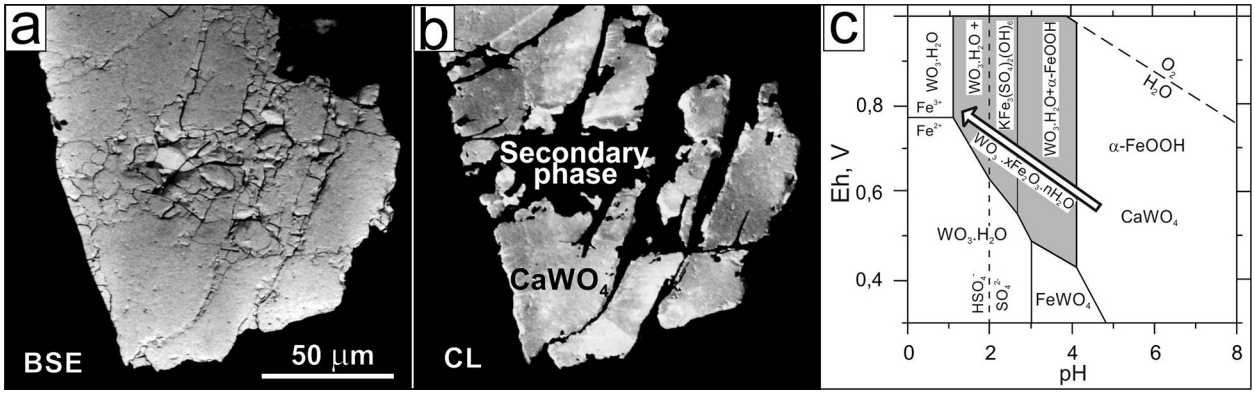

Fig. 2. (a) and (b) pseudomorphic replacement of scheelite by secondary $WO_3.xFe_2O_3.nH_2O$ material (iron-containing meymacite) in an acid medium enriched with Fe ions (images in backscattered electrons (a) and cathode luminescence (b)); (c) Eh–pH diagram with outlined (shaded) areas corresponding to the conditions of alteration scheelite via a pseudomorphic replacement by $WO_3.xFe_2O_3.nH_2O$.

first part. The spongy aggregates are macroscopically white or light-yellow. The Raman spectra of all meymacite varieties including the spongy aggregates are very similar – they are composed of broadened peaks in the whole studied spectral range 100–1050 cm^{-1} (Fig. 3c), and correspond well to the Raman spectra of crystalline $WO_3.1/3H_2O$ (S.G. Fmm2, a=7.359 Å, b=12.513, c=7.704) [19, 20].

The TEM investigation reveals that that the spongy aggregates are the most structurally ordered part of the meymacite. It is found that every single spongy particle represents a thin quasi-crystal consisting of coalesced elongated nanocrystals with length of 20–25 nm and width of 2–3 nm (Fig. 4). The single crystal type of electron diffraction patterns from a spongy particle was obtained only using the convergent beam electron diffraction (CBED) method (Fig. 4a see the insert). The corresponding high resolution (HR) image with two-dimensional lattice fringes is shown in Fig. 4b. The recorded CBED pattern is actually a superposition of several patterns slightly rotated relative to each other, which hinders accurate measurement of d-spacing and reliable zone and phase identification. The HR image shows that the nanocrystals constituting the spongy particle are not ideally stacked – there are some angle discordances and displacements between the atomic planes of neighbor nanocrystals (Fig. 4b). For a more precise determination of the d-spacings, a Fast Fourier Transform (FFT) of the HR image was performed (Fig. 4b). The final measured d-spacings are: 3.85 Å (perpendicularly to the elongation of the particle) and 3.68 Å (in parallel to the elongation of the particle). These d-spacings

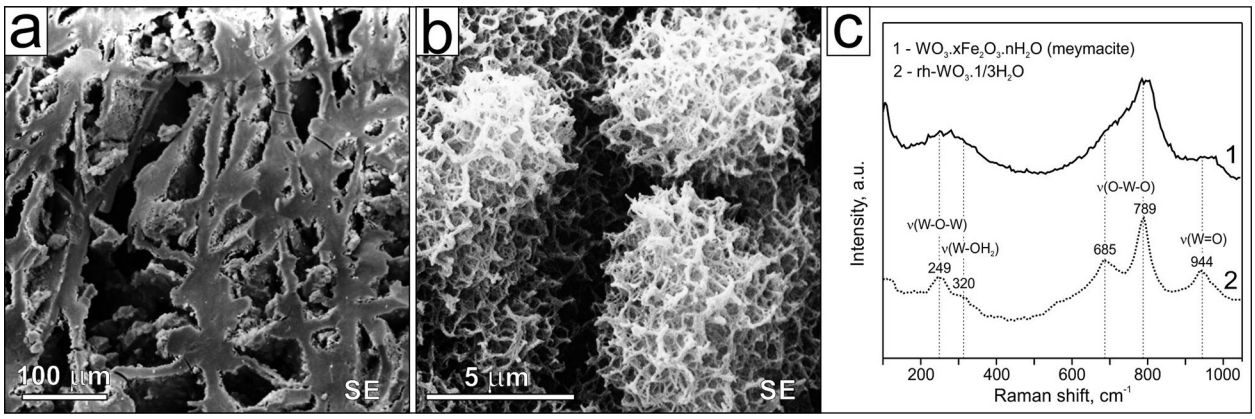

Fig. (3). (a and b) two parts of the iron-containing meymacite with atomic ratio Fe/W ~0.3: massive glassy one (a) and spongy aggregates in cavities of the first part (b); (c) unpolarized Raman spectra of the studied meymacite (1) and crystalline rh-$WO_3.1/3H_2O$ (2).

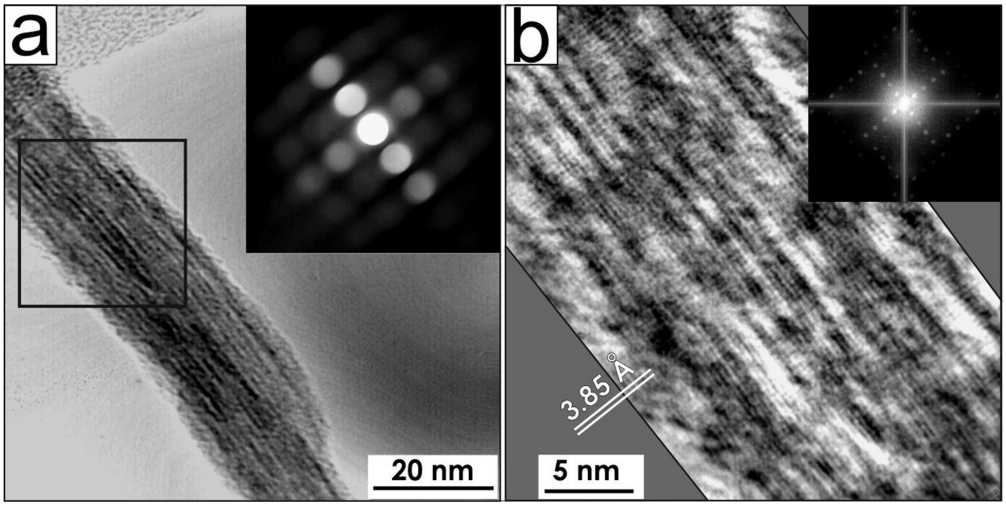

Fig. 4. (a) TEM bright-field image of a single spongy particle of iron-containing meymacite and corresponding convergent beam electron diffraction (CBED) pattern in the insert; (b) high-resolution (HR) image of the area outlined in (a) visualizing fragmented two-dimensional lattice fringes with d-spacings 3.85 and 3.68 Å and corresponding FFT image in the insert.

correspond to [010] zone of $WO_3.1/3H_2O$ (Fmm2): d_{002} = 3.852 Å and d_{200} = 3.680 Å. No other larger d-spacings typical for $WO_3.1/3H_2O$ (Fmm2) as d_{111} = 4.897 Å and d_{020} = 6.257 Å were found in the material under study. The reason for this is in the specific morphology of the studied nanocrystals and the manner of their stacking in the spongy particles. The nanocrystals are very narrow (~2 nm) and elongated (~20 nm) in the [001] direction and across to the elongation may accommodate to 2 unit cells only, as the b parameter of $WO_3.1/3H_2O$ is equal to 1.25 nm. The structure of $WO_3.1/3H_2O$ [20] consists of layers of WO_6 octahedra sharing their corners and forming six-membered rings typical for hexagonal WO_3 and hexagonal tungsten bronzes (HTB). The stacking of the layers is along the [001] direction, every layer being shifted by a/2 relative to the adjacent layer. In the [010] direction there is an alternation of more dense layers of WO_6 shared their corner according to the ReO_3 structure type and layers with two times fewer WO_6 octahedra [20]. Our experimental data (Fig. 4b) provide evidence that the $WO_3.1/3H_2O$ nanocrystals are stacked to each other by connecting their most dense (010) atomic planes. This stacking well explains the observed morphology of the spongy quasi-crystals (Fig. 4a) – they are very thin in the [010] direction and very long in the [001] direction of $WO_3.1/3H_2O$. Because the nanocrystals contain Fe^{3+}, their formula, in analogy with hydrokenoelsmoreite, can be presented as $(W, Fe^{3+})(O,OH)_3.1/3H_2O$.

The obtained results well corresponds to our earlier TEM studies of the structural and orientation relationships between $CaWO_4$ and $WO_3.1/3H_2O$ during the decomposition of $CaWO_4$ in dilute solutions of sulfuric acid at 120°C [21]. It was shown in [22] that the transformation of $CaWO_4$ into $WO_3.1/3H_2O$ is topotactic one. The transformation is most intensively carried out along the {101} planes of $CaWO_4$, which to a greater extent predetermines the formation of $WO_3.1/3H_2O$ nanocrystals elongated in [001] direction.

Tungstite, $WO_3.H_2O$, and *hydrotungstite, $WO_3.2H_2O$,* are rare secondary tungsten minerals in the oxidation zone of the Grantcharitza deposit (Fig. 5a, b). The field ($WO_3.H_2O$ + Fe^{3+}) in the Eh-pH diagram (Fig. 2c) seems to realistically represent the strongly acid (pH≤1) conditions of crystallization of two tungsten trioxide hydrate minerals in the supergene media enriched with iron ions. We have nowhere observed that the two minerals directly replace the primary scheelite – in all examined samples, these minerals occur with iron-containing meymacite and are formed at the expense of meymacite. The hydrotungstite occurs as bright-yellow aggregates in cavities of meymacite. The individual crystals are with size to 50–60 μm. Twins and intergrowths are very common (Fig. 5a). In SEM, the mineral is easily distinguished by desiccation fissures in the crystals due to evaporation of a part of the structural water. The tungstite is fine-crystalline (<10 μm) (Fig. 5b). The mineral is represented by bright-yellow platy crystals and without complex twining. The presence of tungstite and hydrotungstite in the oxidation zone of the deposit indicates that the supergene processes occur in a relatively wide temperature range, because tungstite crystallizes at ≥50°C and hydrotungstite – at ≤50°C.

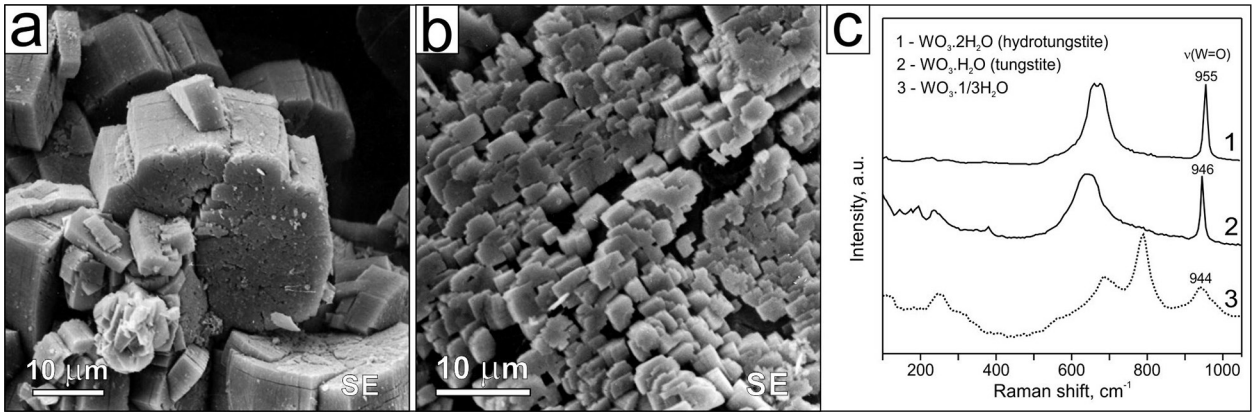

Fig. 5. (a) twinned crystals of hydrotungstite, $WO_3.2H_2O$, in cavity of meymacite; (b) platy crystals of tungstite covering quartz in close proximity to meymacite; (c) unpolarized Raman spectra of $WO_3.nH_2O$ phases (n=2, 1, 1/3)

The structures of the two minerals [23, 24] consist of layers of WO_5OH_2 octahedra sharing their 4 corners in a manner typical of the ReO_3 structure. The two other corners of the octahedra are occupied by non-shared oxygen (terminal W=O bond) and water molecule (W-OH_2 bond). In tungstite, the layers are connected by hydrogen bonds. In the structure of hydrotungstite, additional water molecules are intercalated between adjacent layers. The Raman spectra of hydrotungstite and tungstite (Fig. 5c) well correspond to the literature data [19].

The considered above consecutive processes, namely, (1) scheelite dissolution, (2) replacement of scheelite by iron-containing meymacite, and (3) crystallization of tungstite and hydrotungstite at the expense of meymacite, proceed in the overall trend of decreasing pH (increasing concentration of H_2SO_4).

In the interaction of natural sulfuric acid with scheelite and other minerals (quartz and microcline), the acidity of the supergene solutions are gradually neutralized with a simultaneous increase in the concentration of potassium and sodium. This is a reason that the further structural and chemical evolution of tungsten mineral forms is realized in the general trend of increasing pH.

Amorphous $WO_3.xFe_2O_3.nH_2O$ gels. This natural amorphous material is described here for the first time. The material is macroscopically light-yellow and can be mistaken for fine-crystalline tungstite and hydrotungstite. It is chemical counterpart of iron-containing meymacite. The material is found in quartz fractures (Fig. 6a) without clear positional connections with scheelite and other secondary tungsten minerals indicating that W and Fe were introduced here by supergene solutions.

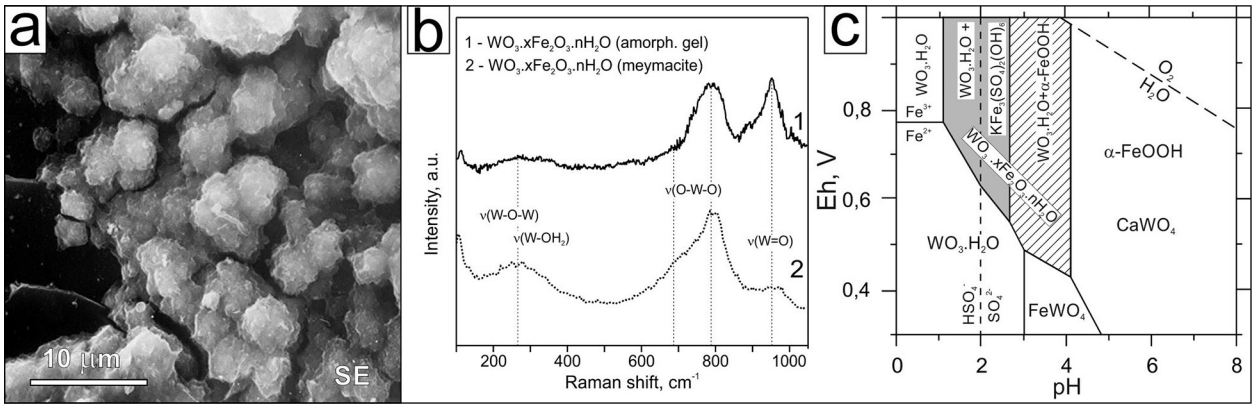

Fig. 6. (a) crust of amorphous $WO_3.xFe_2O_3.nH_2O$ gels on the surface of quartz; (b) Raman spectra of $WO_3.xFe_2O_3.nH_2O$ gel and meymacite; (c) Eh-pH diagram with shaded area corresponding to the most probable gel formation conditions (the hatched area represents less probable conditions).

Dissolution of either tungstite and hydrotungstite or iron-containing meymacite by a supergene solution, followed by transport and a sol-gel process could produce such a type of natural amorphous gels. Dissolution of scheelite can also be a possible source of tungsten in the solution. Normally the gel is accompanied by jarosite, $KFe_3(SO_4)_2(OH)_6$), therefore the field ($WO_3.H_2O$ + $KFe_3(SO_4)_2(OH)_6$) in the Eh–pH diagram (Fig. 6c) can be considered as an approximation to the material formation conditions but keeping in mind that the gel is amorphous.

The Raman spectrum of the studied gel differs significantly from that of the iron-containing meymacite (Fig. 6b). The peak at 950 cm^{-1} corresponding to W=O terminal bond in the gel spectrum has a much higher intensity as is typical for amorphous WO_3 materials/films obtained in various ways including sol-gel process [25, 26] and reflects a significant role of the surface W=O bonds in the tungsten-oxygen clusters composing the materials. In the spectral range 650–850 cm^{-1} corresponding to the stretching vibration of W-O bonds in WO_3 compounds [19], the spectrum of the gel demonstrates a relatively narrow intense peak at 780 cm^{-1} (Fig. 6b). This peak may indicate that the gel clusters are compact and consist of WO_6 octahedra sharing not only their apexes but also edges. This suggestion to a greater extent is confirmed in [27] where radial distribution function (RDF) analysis made for amorphous $WO_3.xFe_2O_3.nH_2O$ gels reveals the presence of a weak peak at 3.2 Å corresponding to W-W nearest-neighbor distance in WO_6 octahedra sharing edges [28] which is typical for polytungstate acid.

Iron-containing hydrokenoelsmoreite $(W,Fe)_2(O,OH)_6.H_2O$ *(ferritugstite)* is the third chemical counterpart of the iron-containing meymacite with the pyrochlore-type structure. The mineral is rare. It sporadically crystalizes in situ in the cavities of meymacite. Macroscopically, it is bright-yellow. The mineral is encountered as well faced octahedral crystals with size 10–20 μm, their twins and intergrowths (Fig. 7a). Besides WO_3, Fe_2O_3 and H_2O, the following chemical components Na_2O, K_2O, CaO and PbO are established in the chemical composition of the mineral. The detailed observation shows that hydrokenoelsmoreite is the result of the interaction of meymacite and supergene solution. This is evidenced by the fact that hydrokenoelsmoreite is formed only there, where there is a meymacite, and the crystallization of hydrokenoelsmoreite is accompanied by the destruction of meymacite – the latter becomes very fragile and friable. The composition of hydrokenoelsmoreite indicates the presence of K, Na, Ca and Pb in the supergene solution. Most likely, this solution contained also W and Fe ions. The ($WO_3.H_2O$+ α-FeOOH) field in Fig. 7c tentatively corresponds to the conditions of crystallization of hydrokenoelsmoreite (pH ~3–4). The proposed pH range is very close to pH of ~3 of the precursor tungsten solutions used for synthesis of the pyrochlore type tungsten trioxide hydrates [29, 30].

The Raman spectrum of hydrokenoelsmoreite (Fig. 7b) is characterized by two broad bands in the spectral ranges 600–750 and 850–1000 cm^{-1} corresponding to symmetric and asymmetric stretching of W-O bonds, respectively [31]. It is notable, that although the mineral is well crystalline, its Raman peaks in the range 600–1000 cm^{-1} are essentially broader than the Raman peaks of the chemical counterparts of the mineral – cryptocrystalline meymacite and amorphous gels. According to [31] broadening of the Raman lines results from structural disorder caused by the presence of iron atoms.

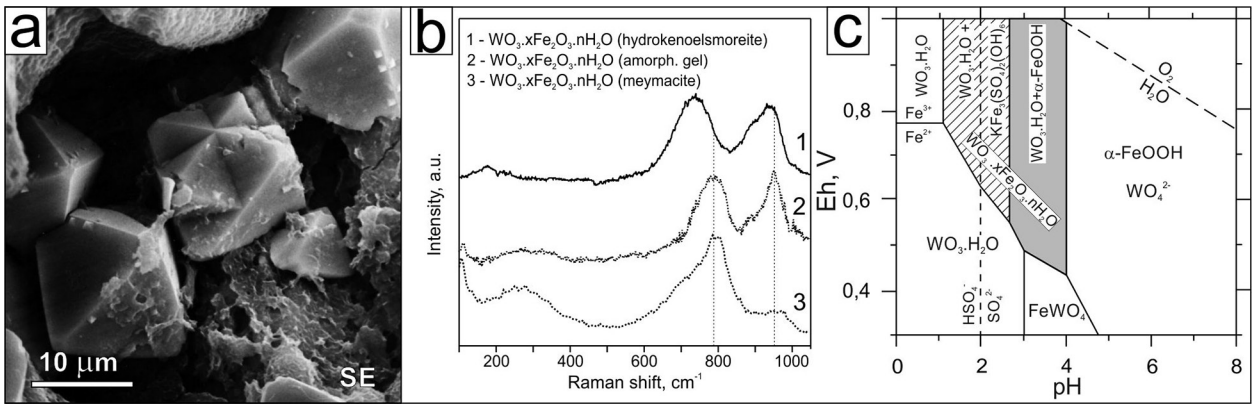

Fig. 7. (a) octahedral crystals and crystal intergrowths of iron-containing hydrokenoelsmoreite in the cavity of iron-containing meymacite; (b) Raman spectra of three $WO_3.xFe_2O_3.nH_2O$ supergene forms of W: hydrokenoelsmoreite, amorphous gel and meymacite; (c) Eh-pH diagram with outlined (shaded) area tentatively corresponding to the hydrokenoelsmoreite formation conditions.

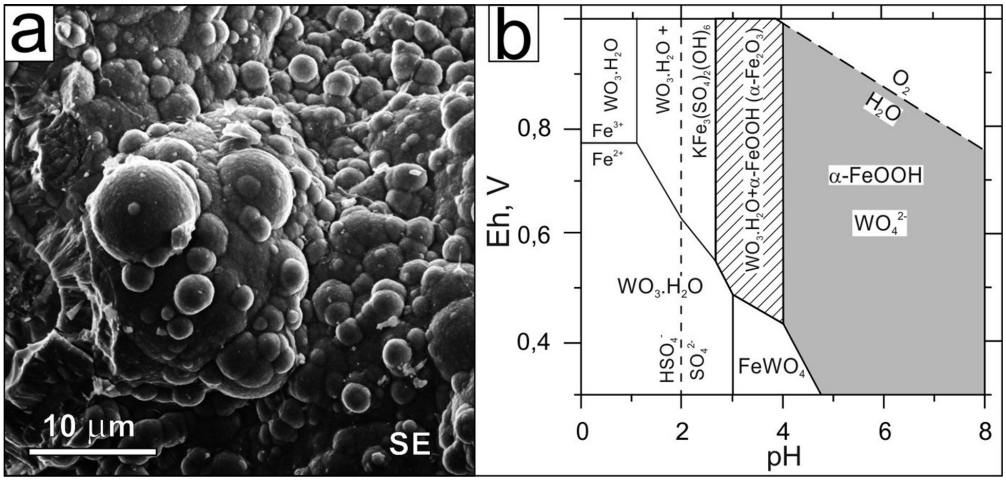

Fig. 8. (a) colloform W-bearing goethite, α-FeOOH, (b) Eh-pH diagram with outlined (shaded) area corresponding to the formation of W-bearing goethite.

Tungsten-bearing goethite, α-FeOOH, is widespread supergene mineral in the oxidation zone of the deposit and most important secondary bearer of tungsten. The mineral is presented by colloform compact mass (Fig. 8a), macroscopically black-colored, filling the fissures and cavities remained after dissolution of scheelite and pyrite, and powder ochreous mass colored in brown to yellow. The established concentration of WO_3 in the goethite aggregates varies in the range 1–10 wt.% [32]. It is shown that to ~2 wt.% of W are structurally incorporated in goethite. The other most enriched in W part of the goethite aggregates is related to a strongly disordered ferrihydrite-like phase (phase Fw) with WO_3 content to 25 wt.%. The presence of tungsten in goethite can be related to two different processes: (1) co-precipitation of Fe and W from colloidal solution causing the formation of colloform goethites, and (2) adsorption of tungsten species by goethite and ferrihydrite. Tungsten adsorption is more extensive at circumneutral pHs of solutions containing monomeric tungstate forms [33]. Tungstate polymerization significantly decreases W adsorption. The (α-FeOOH+WO_4^{2-}) field in Fig. 8b seems to be a reasonable approximation to the conditions of formation W-bearing goethite (pH>4).

Tungsten-bearing hematite α-Fe_2O_3 occurs rarely in local places of compact tungsten-bearing goethite and is characterized by a content of WO_3 of 0.5–2.0 wt.% corresponding to the structural incorporation of W in hematite [32]. The hematite crystallizes via a multistage process including dissolution of goethite, reprecipitation of the material in the form of tungsten-bearing ferrihydrite and subsequent solid-state conversion of ferrihydrite into hematite. According to [34] in both hematite and goethite the structural incorporation of W is realized via protonation scheme: $3Fe^{3+} = W^{6+}+3H^{+}+2\square^{0}$. Similarly to the goethite, the (α-FeOOH+WO_4^{2-}) field in Fig. 8b is an approximation to the conditions of formation W-bearing hematite (pH>4).

Amorphous tungsten-containing $SiO_2.xAl_2O_3.yFe_2O_3.nH_2O$ gel is widespread undefined product of sol-gel processes taken place in the oxidation zone. It is commonly presented by surface yellow-brawn powdery materials with variable content of Fe_2O_3 and WO_3 (to 2 wt.%). The field (α-FeOOH + WO_4^{2-}) outlined in the pH-Eh diagram in Fig. 8c corresponds to the possible conditions for the gels formation. The presence of W in the gel most probably is due to adsorption of monotungstate WO_4^{2-} ions.

Stolzite, $PbWO_4$, and colloform scheelite, $CaWO_4$, are rarely occurred supergene forms of W in the deposit. The field ($CaWO_4$ + α-FeOOH) in the pH-Eh diagrams (Figs. 2c, 6c) well defines conditions of crystallization of these minerals.

CONCLUSIONS

A relatively simple mineral composition of primary ores in the Grantcharitza deposit, strongly dominated by pyrite and scheelite, creates a very wide diversity of secondary W minerals and secondary mineral bearers of W in the oxidations zone in the southern part of the Grantcharitza-Center section. The processes are carried out over a wide range of pH, high oxidation potential Eh corresponding to that characteristic of the waters which are in direct contact with atmospheric oxygen, and with a very important role of Fe^{3+}. In fact, the most important

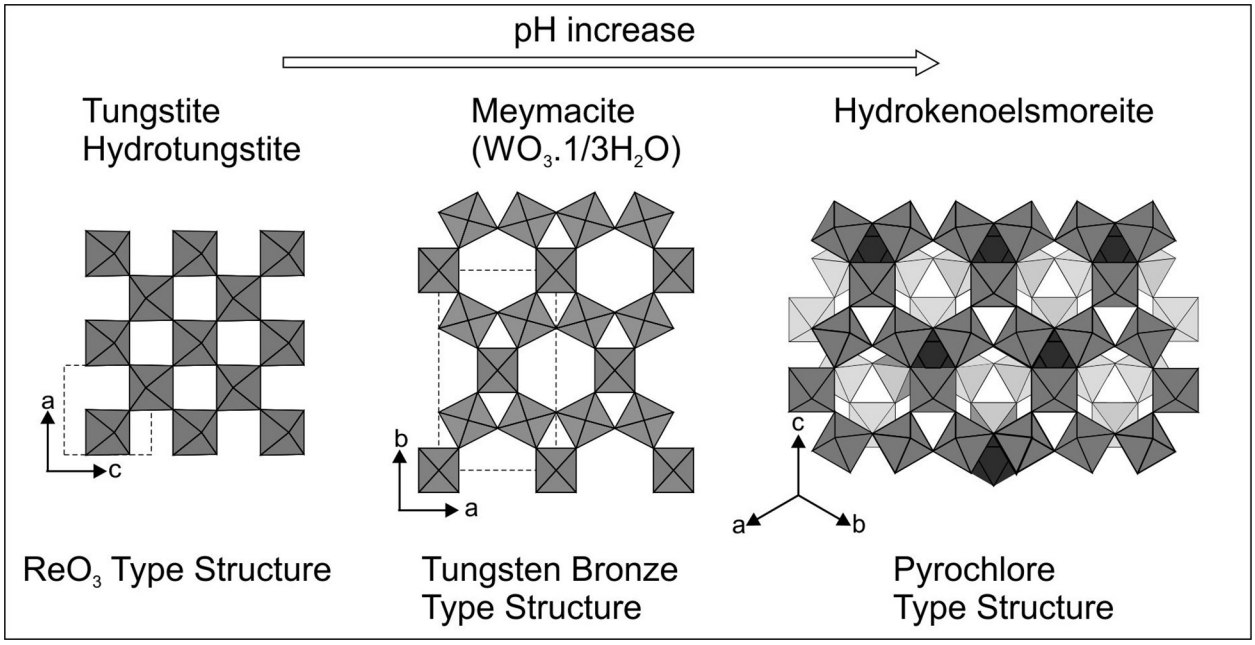

Fig. 9. Summary scheme: dependence of the structure type of secondary tungsten mineral on the pH of solution in the presence of iron ions.

secondary W mineral forming processes in the deposit are realized within the WO_3–Fe_2O_3–H_2O system. These processes are carried out *in situ* and *ex situ* with involving the ground waters and essential transport of dissolved W including its polytungstate ion forms.

Two principal trends of structural and chemical evolution of mineral forms of W are distinguished in the oxidation zone of the deposit. The first trend concerns the processes that occur when the overall pH of supergene solutions decrease. The first group of processes include: (1) dissolution of scheelite accompanied by the formation of polytungstate ions in the solution at pH ~6–4; (2) pseudomorphic replacement of scheelite by poorly crystalline $WO_3.xFe_2O_3.nH_2O$ (iron-containing meymacite) at pH ~4–1; (3) crystallization of tungstite, $WO_3.H_2O$, and hydrotungstite, $WO_3.2H_2O$, at the expense of meymacite at pH <1. It is shown that the most ordered part of the meymacite is represented by nanocrystals with a structure of $WO_3.1/3H_2O$ (Fmm2).

The second group of processes proceeds in the overall trend of increasing pH of supergene solutions and includes: (1) partial dissolution of meymacite upon increasing the pH and the K, Na and W content in the supergene solution (pH ~1–3); (2) occasionally, precipitation of amorphous gels $WO_3.xFe_2O_3.nH_2O$ – chemical counterparts of meymacite, commonly accompanied by jarosite, $KFe_3(SO_4)_2(OH)_6$ (pH ~1–3); (3) crystallization of iron-containing hydrokenoelsmoreite, $(W,Fe)_2(O,OH)_6.H_2O$ – the second chemical counterpart of meymacite with the pyrochlore structure type, as result of the interaction of meymacite and supergene solution enriched with K, Na and Ca and most likely containing W and Fe ions at pH ~3–4; (4) formation of mineral bearers of tungsten: goethite, α-FeOOH, hematite, α-Fe_2O_3, undefined amorphous $SiO_2.xAl_2O_3.yFe_2O_3.nH_2O$ gels, and very rarely of tungstate minerals – supergene scheelite, $CaWO_4$, and stolzite, $PbWO_4$, at pH>4.

Based on the data obtained for the oxidation zone of the Grantcharitza deposit, the authors propose the following summary scheme describing the dependence of the structure type of the secondary tungsten mineral on the pH of the solution in the presence of iron ions (Fig. 9). The increase of pH of the solution is accompanied by the consecutive change of the structure types: ReO_3 type (ReO_3-type layers in the structures of tungstite and hydrotungstite), hexagonal tungsten bronze type (HTB) (HTB-type layers in the structure of $WO_3.1/3H_2O$, meymacite), and pyrochlore type (structure of hydrokenoelsmoreite). According to this scheme, it becomes more apparent the conditions of formation of such tungsten minerals as pittongite and phyllotungstite [3, 4] with combined pyrochlore and tungsten bronze types of structure.

REFERENCES

1. Th. G. Sahama, *Mineral. Rec*, **12**, 81 (1981).
2. P. A. Williams, P. Leverett, J. L. Sharpe, D. M. Colchester, J. Rankin, *Can. Mineral.*, 43, 1061 (2005).

3. I. E. Grey, W. D. Birch, C. Bougerol, S. J. Mills, *J. Solid State Chem.*, **179**, 3860 (2006).
4. W. D. Birch, I. E. Grey, S. J. Mills, C. Bougerol, A. Pring, S. Ansermet, *Can. Mineral.*, **45**, 857 (2007).
5. M. Figlarz, *Prog. Solid State Chem.*, **19**, 1 (1989).
6. M. P. Tarassov, *Geochem. Mineral. Petrol., Sofia*, **30**, 19(1995).
7. A. Koutsospyros, W. Braida, C. Christodoulatos, D. Dermatas, N. Strigul, *J. Hazard Mater.*, **136**, 1 (2006).
8. R. L. Seiler, K. G. Stollenwerk, J. R. Garbarino, *Appl. Geochem.*, **20**, 423 (2005).
9. B. Kamenov, I. Peytcheva, L. Klain, K. Arsova, Y. Kostitsin, E. Salnikova, *Geochem. Miner. Petrol.*, *Sofia*, **36**, 3 (1999).
10. R. M. Garrels, Ch. L. Christ, Solutions, Minerals and Equilibria, Harper & Row Publishers, New York, 1965.
11. A. G. Bulah, K. G. Bulah, Physicochemical properties of minerals and components of hydrothermal solutions. Nedra, Leningrad, 1978.
12. S. Crouch-Baker, P. G. Dickens, S.A. Kay, *J. Chem. Thermodyn*., **17**, 797 (1985).
13. J. B. Brown, *Miner. Depos*., **6**, 245 (1971).
14. L. K. Yahontova, A. P. Grudev, Supegene zone of ore deposits, Publishing House of the Moscow University, Moscow, 1978.
15. K. I. Marinakis, G. H. Kelsall, *Colloids Surf.*, **25**, 369 (1987).
16. M. V. Mohosoev, N. A. Shevtsova, Molybdenum and tungsten speciation in aqueous solutions, Buryat Publishing House, Ulan-Ude, 1977.
17. M. T. Pope, Heteropoly and Isopoly oxometalates (Inorganic Chemistry Concepts, vol. 8), Springer Verlag, Berlin, 1983.
18. G. W. Scherer, *J. Non-Cryst. Solids*, **100**, 1–3, 77 (1988).
19. M. F. Daniel, B. Desbat, J. C. Lassegues, *J. Solid State Chem.*, **67**, 235 (1987).
20. B. Gerand, G. Nowogrocki, M. Figlarz, *J. Solid State Chem.*, **38**, 312 (1981).
21. M. P. Tarassov, V. Dimov, N. Khaltakova, *Comp. rend. Acad. bulg. Sci.*, **51**, 11–12, 65 (1998).
22. M. P. Tarassov, N. Khaltakova, *Comp. rend. Acad. bulg. Sci.*, **52**, 1–2, 61 (1999).
23. J. T. Szimanski, A. C. Roberts, *Can. Mineral.*, **22**, 681 (1984).
24. B. Von Krebs, *Acta Cryst.*, **B28**, 2222 (1972).
25. A. Chemseddine, M. Henry, J. Livage, *Rev. Chim. miner.*, **21**, 487 (1984).
26. Y. A. Yang, J. N. Yao, *J. Phys. Chem. Solids*, **61**, 647 (2000).
27. N. S. Zotov, M. P. Tarassov, *Mater. Sci. Forum*, **133–136**, 945 (1993).
28. T. Nanba, S. Takano, I. Yasui, T. Kudo, *J. Solid State Chem.*, **90**, 47 (1991).
29. J. R. Günter, M. Amberg, H. Schmalle, *Mat. Res. Bull*., **24**, 289 (1989).
30. A. Coucou, M. Figlarz, *Solid State Ionics*, **28–30**, 1762 (1988)
31. M. P. Tarassov, M. S. Marinov, L. L. Konstantinov, N. S. Zotov, *Phys. Chem. Miner*., **21**, 1/2, 63 (1994).
32. M. Tarassov, B. Mihailova, E. Tarassova, L. Konstantinov, *Eur. J. Mineral.*, **14**, 977 (2002).
33. J. Sun, B. C. Bostick, *Chem. Geol*., **417**, 21 (2015).
34. S. Kreissl, R. Bolanz, J. Göttlicher, R. Steininger, M. Tarassov, G. Markl, *Am. Mineral.*, **101**, 2701 (2016).

СТРУКТУРНА И ХИМИЧНА ЕВОЛЮЦИЯ НА МИНЕРАЛНИ ФОРМИ НА ВОЛФРАМА В ОКИСЛИТЕЛНАТА ЗОНА НА НАХОДИЩЕ ГРЪНЧАРИЦА (ЗАПАДНИ РОДОПИ, БЪЛГАРИЯ)

М. П. Тарасов*, Е. Д. Тарасова

Институт по минералогия и кристалография „Академик Иван Костов“, Българска Академия на науките, ул. Акад. Георги Бончев, бл. 107, 1113 София, България

Постъпила март, 2018 г.; приета май, 2018 г.

(Резюме)

Две основни тенденции на структурната и химична еволюция на минералните форми на W са проявени в зоната на окисление на шеелит-пиритовото ($CaWO_4$–FeS_2) находище Грънчарица. Първата тенденция е свързана с процесите, които протичат при общо намаляване на pH на супергенните разтвори. Най-ранният процес включва взаимодействие на първичния шеелит със супергенния разтвор, което води до: (а) разтваряне на минерала, придружено от образуване на поливолфраматни йони в разтвора при pH ~6–4, и (б) псевдоморфно заместване на минерала от криптокристален $WO_3.xFe_2O_3.nH_2O$ (желязо-съдържащ меймацит) при pH ~4–1. Показано е, че най-подредената част на меймацита е представена от удължени нанокристали със структура на $WO_3.1/3H_2O$ (Fmm2). При pH<1 за сметка на меймацита се формират тунгстит, $WO_3.H_2O$, и хидротунгстит, $WO_3.2H_2O$. Втората група процеси протича при обща тенденция на повишаване на pH на супергенните разтвори. При повишаване на pH и съдържанието на K и Na в супергенния разтвор меймацитът частично се разтваря и волфрамът преминава в разтвор и в други вторични фази. В някои случаи разтворените волфрам и желязо се утаяват, образувайки аморфни гели $WO_3.xFe_2O_3.nH_2O$ – химични аналози на меймацит, обикновено придружени от ярозит, $KFe_3(SO_4)_2(OH)_6$ (pH ~1–3). Взаимодействието на такъв разтвор с меймацит при pH ~3–4 води до частичното или почти пълното разтваряне на меймацита и кристализация на втория химичен аналог на меймацит – желязо-съдържащ хидрокеноелсмореит, $(W,Fe)_2(O,OH)_6.H_2O$, с пирохлоров тип структура. При pH> 4 основните носители на волфрама стават гьотитът α-FeOOH (най-широко разпространен минерал), хематитът α-Fe_2O_3 и аморфните $SiO_2.xAl_2O_3.yFe_2O_3.nH_2O$ гелове. В редки случаи в тези условия се формират супергенен шеелит, $CaWO_4$, и щолцит, $PbWO_4$. На базата на получените данни е предложена обобщена схема за зависимостта на структурния тип на вторичния волфрамов минерал от pH на разтвора в присъствието на железни йони. При нарастване на pH от <1 до 4 настъпва последователна смяна на следните структурни типове: тип ReO_3 (слоеве от ReO_3-тип в структурите на тунгстит и хидротунгстит), тип хексагонален волфрамов бронз (HTB) (HTB-тип слоеве в структурата на $WO_3.1/3H_2O$, меймацит) и тип пирохлор (структура на хидрокеноелсмореит).